

QUANTUM DEGENERACY IN LITHIUM GASES

RANDALL G. HULET and JORDAN M. GERTON

Rice University

Department of Physics and Astronomy, MS61

Houston, TX 77251, USA

1. Introduction

Lithium is an attractive atom for studies of quantum degenerate gases because its two naturally occurring isotopes, ^6Li and ^7Li , have opposite exchange symmetry and have stable nuclei. Since ^6Li is composed of an odd number of spin-1/2 particles (3 electrons, 3 protons, 3 neutrons), it is itself a half-integer composite particle obeying Fermi-Dirac statistics. On the other hand, ^7Li with its extra neutron is a composite boson. The phenomena exhibited by each isotope, therefore, should be vastly different at ultra-low temperatures, where effects of quantum degeneracy are manifested. For example, we have shown that ^7Li undergoes Bose-Einstein condensation (BEC) [1], the paradigm of all quantum statistical phase transitions. A gas of ^6Li , conversely, cannot directly Bose condense, although they can undergo a BEC-like phase transition in which particles form ‘Cooper pairs’. This effect is responsible for electronic superconductivity and for superfluidity of ^3He .

In this chapter, we describe our experiments with ultracold lithium atoms. These experiments include the first direct observation of the growth and collapse of a condensate with attractive interactions, molecular spectroscopy of a Bose-Einstein condensate, and sympathetic cooling of ^6Li atoms by ^7Li atoms.

2. Interactions in Dilute Gases

One of the primary reasons for the intense interest in dilute Bose-Einstein condensates is that the interactions are weak, which facilitates comparison between theory and experiment. A great simplification arises because the density of trapped gases is usually low enough that three-body interactions can be ignored, and

the two-body interaction potentials of the alkali-metal atoms have been determined quite accurately in recent years by photoassociative spectroscopy (Section 2.2). Furthermore, at ultra-low temperatures the de Broglie wavelength Λ is much longer than the characteristic two-body interaction length, which is typically only a few nanometers. When this is the case, the effect of the interaction can be represented by a single parameter, the *s*-wave scattering length a [2]. The magnitude of a indicates the strength of the interaction, while the sign determines whether the interactions are effectively attractive ($a < 0$) or repulsive ($a > 0$). The "diluteness parameter", $n|a|^3$, where n is the density, ranges from about 10^{-8} to 10^{-4} in all the alkali BEC experiments. This parameter may be a somewhat smaller for the hydrogen BEC experiment [3], due to its much smaller scattering length.

2.1. MEAN-FIELD THEORY

The effects of interactions on the condensate have been studied using mean-field theory [4]. In this approximation, the exact, many-body interaction Hamiltonian is replaced by its mean value, resulting in an interaction energy $U = 4\pi\hbar^2 an/m$, where m is the atomic mass [2]. For a gas at zero temperature, the net result of the interactions and the confining potential can be found by solving the non-linear Schrödinger (Gross-Pitaevskii) equation for the wave function of the condensate, $\psi(r)$:

$$\left(-\frac{\hbar^2}{2m} \nabla^2 + V(r) + U(r) - \mu \right) \psi = 0 \quad (1)$$

Here μ is the chemical potential, and $V(r)$ is the confining potential provided by the trap. In a spherically symmetric harmonic trap with oscillation frequency ω , $V(r) = \frac{1}{2}m\omega^2r^2$. The interaction energy $U(r)$ is determined by taking $n(r) = |\psi(r)|^2$.

2.2. PHOTOASSOCIATIVE SPECTROSCOPY

The interaction potentials for hydrogen and the alkali-metal atoms are all qualitatively the same, in that they have a repulsive inner-wall, a minimum that supports vibrational bound states (except for the triplet potential of hydrogen), and a long-range van der Waals tail. Their respective scattering lengths, however, differ enormously in magnitude and in sign. This variation arises because of differences in the proximity of the least-bound vibrational state to the dissociation limit. As with the familiar attractive square-well potential, a barely bound or barely unbound state leads to collisional resonances that produce very large magnitude scattering lengths. Small changes in the interaction potential, therefore, may result in a large change in the magnitude, or even a change of the sign of a . A difference in mass, even when the interaction potential is the same, will give entirely different scattering lengths, as is the case with ${}^6\text{Li}$ and ${}^7\text{Li}$. In the past few years, photoassociative

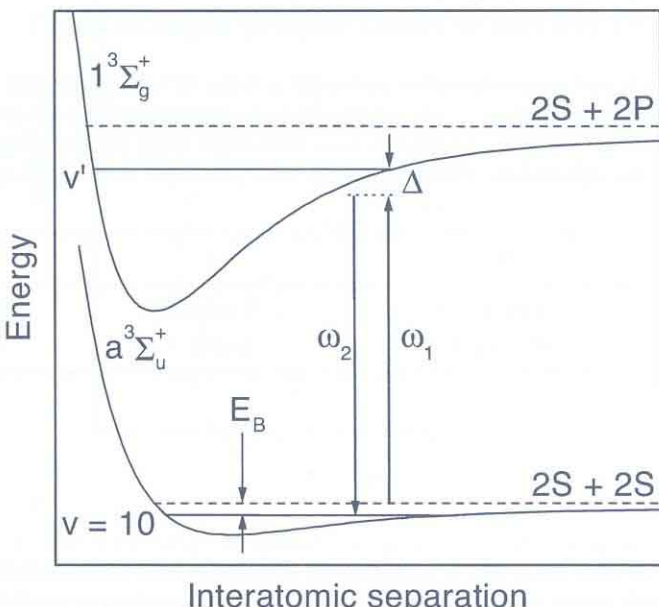


Figure 1. Schematic diagram of two-photon photoassociation. (Reprinted from Ref. 39 by permission from Nature, copyright 2000, Macmillan Magazines Ltd.)

spectroscopy of ultracold atoms has proven to be the most precise method for determining scattering lengths [5]. In one-photon photoassociation, a laser beam is passed through a gas of ultracold atoms confined to a trap. As the laser frequency is tuned to a free-bound resonance, diatomic molecules are formed resulting in a detectable loss of trapped atoms. Since the intensity of the trap-loss signal is sensitive to the ground-state wavefunction, useful information about the ground-state interaction potential is obtained. The value of the scattering length is found by numerically solving the Schrödinger equation using the potential. This method has been used to find the scattering lengths for Li, Na, K, and Rb [5].

A more precise method for finding scattering lengths is to probe the ground state molecular levels directly since they are extremely sensitive to the binding energy of the least-bound molecular state. We have used two-photon photoassociation, as shown in Fig. 1, to directly measure this binding energy for both stable isotopes of lithium, the bosonic isotope ^7Li [6] and the fermionic isotope ^6Li [7]. In this method, a laser is tuned to near the free-bound transition as in one-photon photoassociation, while the frequency of a second laser is tuned to resonance between the bound excited state and a bound ground state. The frequency difference between the two lasers gives the binding energy directly. This technique has resulted in the most precisely known atomic potentials. Table I gives the triplet and singlet scattering lengths for both isotopes individually, as well as for mixed isotope interactions [7]. Two-photon spectroscopy of the ground-state

has also been used recently to find the scattering lengths of Rb [8].

TABLE I. Triplet and singlet scattering lengths in Bohr, for isotopically pure and mixed gases of lithium. The singlet scattering lengths were determined from one-photon photoassociative spectra, while the triplets were determined using the two-photon Raman technique. The mixed case scattering lengths were calculated from the ${}^6\text{Li}_2$ and ${}^7\text{Li}_2$ potentials.

	${}^6\text{Li}$	${}^7\text{Li}$	${}^6\text{Li} / {}^7\text{Li}$
a_T	-2160 ± 250	-27.6 ± 0.5	40.9 ± 0.2
a_S	45.5 ± 2.5	33 ± 2	-20 ± 10

2.3. IMPLICATIONS OF $a < 0$

For a repulsive gas ($a > 0$), a condensate will be stable and its thermodynamic properties, such as its critical temperature T_c or its elementary excitation spectra, can be calculated by a perturbation expansion in the small parameter na^3 [2]. For $a < 0$, however, the situation is very different. Since U decreases with increasing n , an untrapped (homogeneous) gas is mechanically unstable to collapse. It was long believed, therefore, that BEC of a gas with attractive interactions is precluded by a conventional phase transition into either a liquid or a solid [9, 10]. We did, however, observe BEC in a gas of ${}^7\text{Li}$ [1]. The condensate occupation number N_0 was observed to be limited to a number well below the total population of atoms in the trap (Section 4.1) [11], in contrast to observations made in a repulsive gas. A numerical solution to Eq. (1) is found to exist only when N_0 is smaller than a limiting value N_m [12]. In effect, the zero-point kinetic energy of trapped atoms provides a stabilizing influence. The limit can be understood as requiring that the interaction energy U be small compared to the trap level spacing $\hbar\omega$, so that the interactions act as a small perturbation to the ideal-gas solution. This condition implies that N_m is of the order $\ell_0/|a|$, where $\ell_0 = (\hbar/m\omega)^{1/2}$ is the length scale of the single-particle trap ground state [13]. It is at first surprising that N_m increases proportional to ℓ_0 , since it is known that BEC cannot occur in a homogeneous gas. However, the density of the condensate, N_0/ℓ_0^3 , tends to zero as $\ell_0 \rightarrow \infty$, and so there is a trade-off between number and density.

The stability of an attractive condensate can be further explored by a variational method [13, 14, 15]. Here the ground-state solution to Eq. (1) is assumed to maintain the Gaussian form of the ideal gas solution, while the variational parameter is the width ℓ of the Gaussian. By substituting this solution into the energy operator given by the first three terms of Eq. (1), an energy functional $H(\ell)$ is obtained. For $N_0 < N_m$, the harmonic trapping potential and the kinetic energy terms produce a local minimum in $H(\ell)$ which supports a metastable condensate,

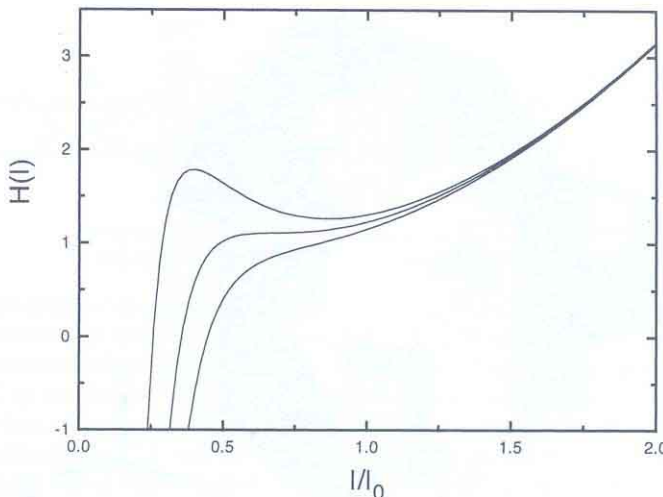


Figure 2. The condensate energy H , plotted in units of $N_0\hbar^2/m\ell_0^2$. The upper curve corresponds to $N_0 = 0.48 \ell_0/|a|$, the middle curve to $N_0 = 0.68 \ell_0/|a|$, and the lower curve to $N_0 = 0.87 \ell_0/|a|$. It is evident that a local minimum in H exists near $\ell = \ell_0$ if N_0 is sufficiently low, indicating that a metastable condensate can exist. (Reprinted from Ref. 13).

as shown in Fig. 2. As N_0 approaches N_m , the attractive interaction term causes the depth of the minimum to decrease until it vanishes entirely for $N_0 > N_m$ [13]. An exact numerical solution to the nonlinear Schrödinger equation, gives a value for N_m of 1250 for ${}^7\text{Li}$ in our trap, while the variational calculation with a Gaussian ansatz gives a result only 15% greater. This is a definite prediction of the mean-field theory that can be quantitatively checked. The results of our measurement of N_m are given in Section 4.1.

3. Apparatus and Methods for Making a BEC

In this section, we describe the main ingredients of the experiment: magnetic trapping, evaporative cooling, phase-contrast imaging, and image analysis.

3.1. MAGNETIC TRAP

The apparatus used to produce BEC of ${}^7\text{Li}$ is described most completely in Ref. [13]. A Zeeman slower is used to slow an atomic beam of lithium atoms, which are then directly loaded into a magnetic trap. There is no magneto-optical trap used in the experiment. The magnetic trap is unique in that it is made from permanent magnets, as shown in Fig. 3 [16]. By exploiting the enormous field gradients generated by rare-earth magnets, the resulting trap potential was made nearly spherically-symmetric with a large harmonic oscillation frequency of ~ 150 Hz. Since N_m is limited by the tightest trap direction [13, 17], the condensate density is

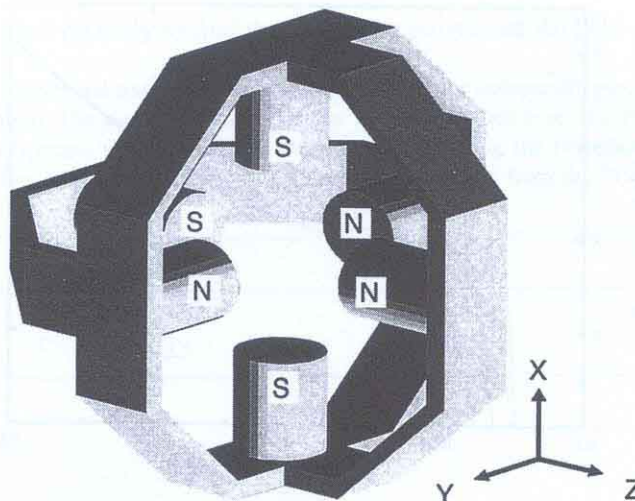


Figure 3. Diagram showing the orientation of the cylindrical trap magnets for the permanent magnet trap. The letters indicate the inner tip magnetizations of the NdFeB cylinder magnets. The tip-to-tip magnet spacing is 4.45 cm. The structure around the magnets is a magnetic stainless steel yoke that supports the magnets and provides low reluctance paths for the flux to follow between opposite signed magnets. (Reprinted from Ref. 16).

maximized for a spherically symmetric potential. By actively stabilizing the temperature of the magnets the fields are made highly stable, allowing for relatively repeatable and stable experimental conditions. The bias field at the center of the trap is 1004 G.

3.2. EVAPORATIVE COOLING

After about 1 s of loading, $\sim 2 \times 10^8$ atoms in the doubly spin-polarized $F = 2$, $m_F = 2$ state are accumulated. These atoms are then laser cooled to near the Doppler cooling limit of $200 \mu\text{K}$. At this number and temperature, the phase space density, $n\Lambda^3$, is still more than 10^5 times too low for BEC. The atoms are cooled further by forced evaporative cooling. The hottest atoms are driven to an untrapped ground state by a microwave field tuned just above the $(F = 2, m_F = 2) \rightarrow (F = 1, m_F = 1)$ Zeeman transition frequency of approximately 3450 MHz. As the atoms cool, the microwave frequency is reduced at a rate which maximizes the phase-space density of the trapped atoms [18]. The optimal frequency vs. time trajectory depends on the elastic collision rate and the trap loss rate. The elastic collision rate $n\sigma v$ is roughly 1 s^{-1} , with cross-section $\sigma = 8\pi a^2 \approx 5 \times 10^{-13} \text{ cm}^2$. The collision rate is approximately constant during evaporative cooling. We have recently measured the loss rate due to collisions with hot background gas atoms to be $< 10^{-4} \text{ s}^{-1}$, and the inelastic dipolar-relaxation collision rate constant to be $1.05 \times 10^{-14} \text{ cm}^3 \text{ s}^{-1}$ [19]. From the low background collision loss rate, we

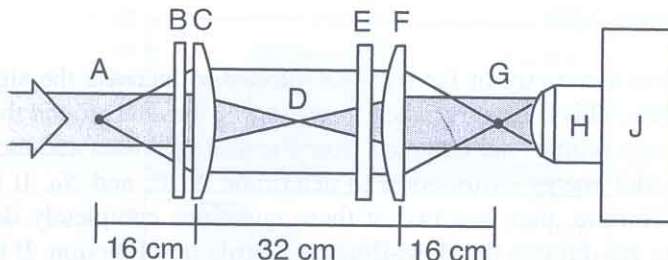


Figure 4. A schematic of the imaging system used for *in situ* phase-contrast polarization imaging. A linearly polarized laser beam is directed through the cloud of trapped atoms located at A. The probe beam and scattered light field pass out of a vacuum viewport B, and are relayed to the primary image plane G by an identical pair of 3-cm-diameter, 16-cm-focal-length doublet lenses C and F. The light is then re-imaged and magnified onto a camera J by a microscope objective H. The measured magnification is 17.5, and the camera pixels are $24 \mu\text{m}$ square. A linear polarizer E is used to cause the scattered light and probe fields to interfere, producing an image sensitive to the refractive index of the cloud. (Reprinted from Ref. 13).

estimate the background gas pressure in the apparatus to be $< 10^{-12}$ torr. Quantum degeneracy is typically reached after 120 seconds, with $N \approx 10^6$ atoms at $T \approx 700$ nK. Lower temperatures are reached by extending the cooling time or by the application of a short, deep microwave quench pulse.

3.3. PHASE-CONTRAST IMAGING

After evaporative cooling, the spatial distribution of the atoms is imaged *in situ* using an optical probe. Since the single-particle harmonic oscillator ground state of our trap has a Gaussian density distribution with a $1/e$ -radius of only $3 \mu\text{m}$, a high-resolution imaging system is required. Because the optical density of the atoms is sufficiently high to cause image distortions when probed by near-resonant absorption [20], we instead use a phase-contrast technique with a relatively large detuning from resonance $\Delta = \pm 250$ MHz. Our implementation of phase-contrast imaging, shown schematically in Fig. 4, is both simple and powerful. It exploits the fact that atoms in a magnetic field are birefringent, so the light scattered by the atoms is polarized differently from the incident probe light. A linear polarizer projects the polarization of the scattered and probe light onto a common axis, which causes them to interfere. Since the phase of the scattered light is equal to $\alpha/4\Delta$, where α is the on-resonance optical density, the spatial image recorded on the CCD camera is a representation of the integrated atomic column density. Phase-contrast polarization imaging is described more fully in Ref. [13].

3.4. DATA ANALYSIS

The cylindrical symmetry of the trap is exploited to increase the signal to noise ratio of the data. This is accomplished by averaging the data around the cylindrical trap axis. Image profiles are obtained from the averaged data and the profiles are fit with a model energy distribution to determine N , T , and N_0 . If the gas is in thermal equilibrium, then any two of these quantities completely determine the density of the gas through the Bose-Einstein distribution function. If the gas is not in thermal equilibrium, such as is the case when the condensate is undergoing the growth/collapse cycles discussed in Section 5, then a more complicated function is required. Using a model based on the quantum Boltzmann equation [21], we find that atoms in lowlying levels quickly equilibrate among themselves and the condensate, and that highenergy atoms are well thermalized among each other. Therefore, a three parameter function that includes two chemical potentials corresponding to these two parts of the distribution, and a temperature representing the high-energy tail of the distribution, is sufficient to describe the expected non-equilibrium distributions and to determine N_0 [22]. The fit yield an average reduced χ^2 of very nearly 1, indicating that the model is consistent with the data within the noise level. The procedure was tested by applying it to simulated data generated by the quantum Boltzmann model, and also by comparing the analysis of experimental images of thermalized clouds using both equilibrium and nonequilibrium models. From these tests, the systematic error introduced by the nonequilibrium model is estimated to be not more than ± 60 atoms. The most significant uncertainty in N_0 is the systematic uncertainty introduced by imaging limitations. While the imaging system is nearly diffraction limited, the resolution is not negligible compared to the size of the condensate, and imaging effects must be included in the fit [20]. Imaging resolution is accounted for by measuring the point transfer function of the lens system and convolving this function with the images. Uncertainties in the resolution lead to a systematic uncertainty in N_0 of $\pm 20\%$ [22].

4. Experimental Results

4.1. LIMITED CONDENSATE NUMBER

Bose-Einstein condensation of a gas with attractive interactions is indeed possible, as can be seen from the images of Fig. 12. These three images correspond to $N \approx 70,000$, but the middle image fits to $N_0 = 1210$ atoms, while the upper image fits to $N_0 = 40$ atoms. The condensate is clearly visible even though $N_0 \ll N$. The excellent signal to noise ratio evidenced here accounts for our high sensitivity to small values of N_0 . In all cases, N_0 is less than 1250 atoms to within the experimental uncertainty, even for N as large as 10^5 atoms. Fig. 5 shows histograms of measurements of N_0 for several delay times following a deep evaporation quench

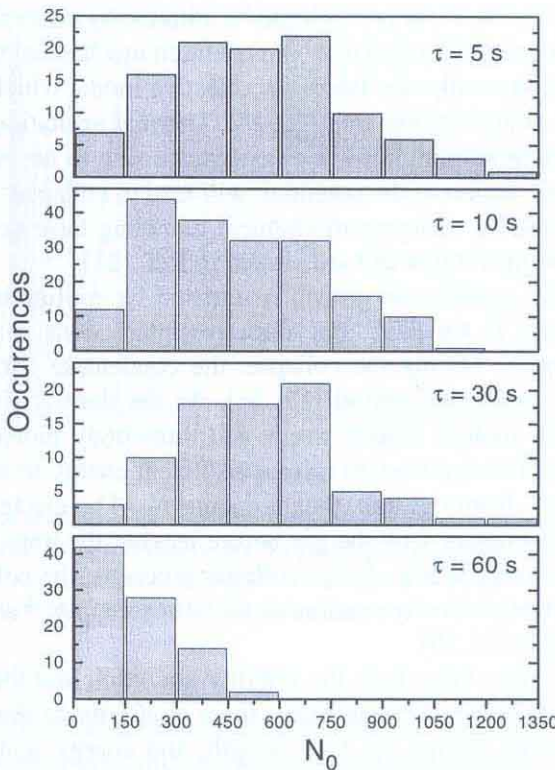


Figure 5. Histograms of condensate occupation number. (Reprinted from Ref. 22).

pulse. These histograms are generated from hundreds of independent measurements of N_0 , each of which is the result of loading the trap, evaporatively cooling the gas, flashing the probe pulse to record a phase-contrast image, and finally, analyzing the image to extract the value of N_0 . These distributions demonstrate the fact that N_0 is limited to a value near 1200 atoms. This value is consistent with, and therefore constitutes a quantitative test of mean-field theory [12].

5. Dynamics of Condensate Growth and Collapse

5.1. THEORY

Given that the condensate is unstable for $N_0 > N_m$, it is natural to ask how this limit is enforced: what happens when atoms are added to the condensate and N_0 grows to near N_m ? Insight into this question can be gained by reference to Fig. 2, which shows an energy barrier in configuration space for $N_0 < N_m$. The relevant coordinate in this figure is the spatial size of the condensate, and changes in this coordinate can be viewed as the motion of a quasi-particle in an effective potential. As N_0 approaches N_m , the condensate becomes unstable to collective

collapse [15, 17, 23, 24, 25, 26], which can be initiated by either thermal excitation over the energy barrier, or by macroscopic quantum mechanical tunneling through it. The condensate has only one unstable collective mode, which is the breathing mode in the case of an isotropic trap [27, 28]. Thermal excitation of the breathing mode with sufficient amplitude for the condensate size to become small enough to sample the inner region of the potential, will lead to collapse. The rates for this thermal process and for quantum mechanical tunneling have been calculated for various relevant temperatures and are plotted in Ref. [21].

Experimentally, condensate growth is initiated by cooling the gas below the critical temperature T_c for BEC. For attractive interactions, N_0 grows until the condensate collapses. During the collapse, the condensate shrinks on the time scale of the trap oscillation period [17, 21]. As the density rises, the rates for inelastic collisions such as dipolar decay and three-body molecular recombination increase [19]. These processes release sufficient energy to immediately eject the colliding atoms from the trap, thus reducing N_0 . The ejected atoms are very unlikely to further interact with the gas before leaving the trap, since the density of noncondensed atoms is low. As the collapse proceeds, the collision rate grows quickly enough that the density remains small compared to a^{-3} and the condensate remains a dilute gas [21, 29].

The physics determining both the stability condition and the dynamical process of collapse of the condensate bears some similarity to that of a star going supernova [30], even though the time, length, and energy scales for these two phenomena are very different. In the stellar case, the stability criterion is provided by a balance between the pressure due to the quantum degeneracy of the electrons within the star and gravitational attraction. If the mass of the star exceeds the stability limit [31], the star collapses, releasing nuclear energy and triggering a violent explosion. In contrast to the stellar case, the condensate regrows after a collapse as it is fed by collisions between thermal atoms in the gas.

Both the collapse and the initial cooling process displace the gas from thermal equilibrium. As long as N_0 is smaller than its equilibrium value, as determined by the total number and average energy of the trapped atoms, the condensate will continue to fill until another collapse occurs. This results in a cycle of condensate growth and collapse, which repeats until the gas comes to equilibrium with some $N_0 < N_m$. Figure 6 shows a typical trajectory of N_0 in time, calculated using the quantum Boltzmann equation, for our experimental conditions [21]. In this calculation we assume that N_0 is reduced to zero when a collapse occurs, on the basis of the model proposed in Ref. [21].

The non-linear Schrödinger equation (Eq. (1)) has been used to describe many wave-collapse phenomena occurring in classical wave physics. Some of these phenomena are the collapse of Langmuir waves in plasmas [32], and self-focusing of light waves propagating in a medium with a cubic non-linearity [33]. Because of this far-ranging applicability there is an extensive literature devoted to the solution

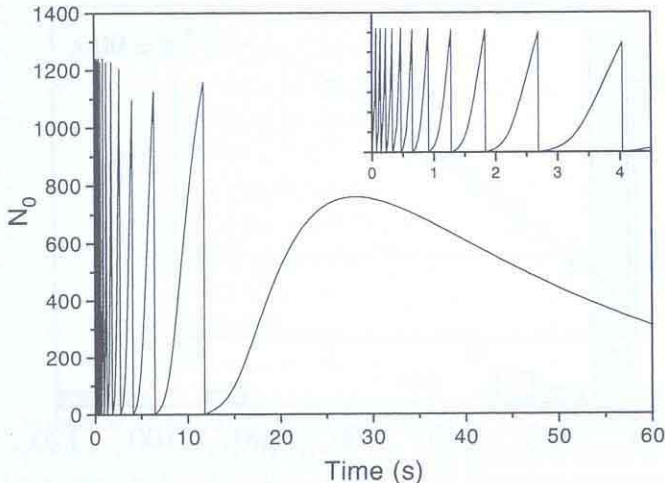


Figure 6. Numerical solution of the quantum Boltzmann equation, showing evolution of condensate occupation number. A trapped, degenerate ^7Li gas is rapidly quenched at $t = 0$ to a temperature of about 100 nK and a total number of 40,000 atoms. The gas then freely evolves in time. The inset shows an expanded view of the early time behavior on the same vertical scale. (Reprinted from Ref. 22).

of the non-linear Schrödinger equation under various conditions. Kagan *et al.* and others have begun to apply some of this accumulated experience to the description of the collapse of a condensate, including both growth and non-linear loss [29, 34]. However, a complete theoretical description of the growth and collapse process, accurate at finite temperature, is an extremely complicated problem that has not yet been fully solved.

5.2. EXPERIMENT

We have obtained indirect experimental evidence for the growth/collapse model, which will be presented in this section. In Section 6.2, we will describe a direct observation of growth/collapse dynamics that was made possible by dumping the condensate using a molecular transition.

Although phase-contrast imaging can in principle be nearly nonperturbative [35], it is not possible to reduce incoherent scattering to a negligible level and simultaneously obtain low enough shot noise to measure small values of N_0 accurately. Each atom therefore scatters several photons during a probe pulse, heating the gas and precluding the possibility of directly observing the evolution of N_0 in time as in Fig. 6. This limitation cannot be overcome by repeating the experiment and varying the delay time τ between the microwave quench pulse and the probe, because the evolution of N_0 is made unrepeatable by random thermal and quantum fluctuations in the condensate growth and collapse processes, as well

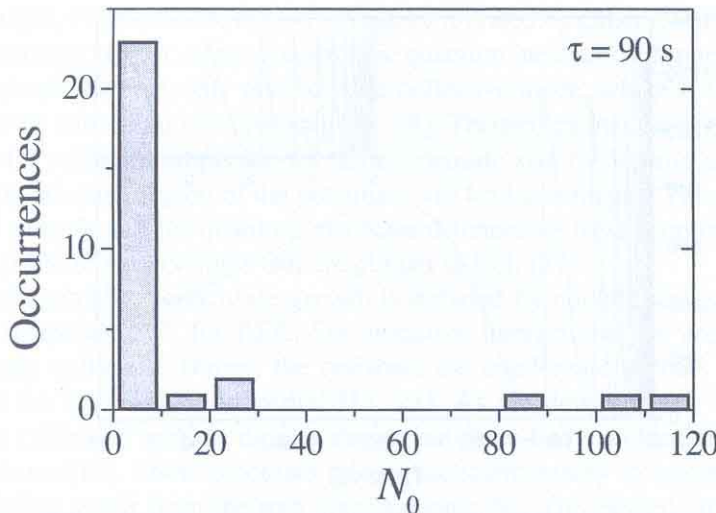


Figure 7. Distribution of condensate number measured for $\tau = 90$ s. No condensate is expected at this long time, so the width of the distribution is a direct measure of the statistical noise. The noise is small compared to the width of the distributions for earlier times, when a condensate is present.

as experimental fluctuations in the initial conditions. Because of this, the values of N_0 occurring at a particular τ are expected to vary as different points in the collapse/fill cycle are sampled. We have observed such variations by measuring N_0 for many similarly prepared samples at several values of τ . The results are the histograms shown in Fig. 5. For small τ , N_0 ranges from near zero to about 1200 atoms, as expected if the condensate is alternately filling to near the theoretical maximum and subsequently collapsing. At having only small N_0 values at $\tau = 60$ s. The variations in N_0 are uncorrelated with changes in N , T , probe parameters, imaging model parameters, and goodness of fit. The statistical noise in our measurement of N_0 is much less than the width of the measured distributions. This is demonstrated by Fig. 7, which shows the histogram corresponding to $\tau = 90$ s, a time sufficiently long that no condensate is expected. The distribution for $\tau = 90$ s, therefore, is a direct measure of the noise in measuring N_0 : ± 60 atoms. Since no other mechanism has been proposed to explain the observed variations in the distributions shown in Fig. 5, we consider the observation of these variations to strongly support the growth/collapse model.

The condensate growth and collapse cycle is driven by an excess of noncondensed atoms compared to a thermal distribution. This excess can be examined directly. From N and T , the critical number for the BEC transition, N_c , is calculated and the ratio N/N_c plotted as a function of delay time in Fig. 8. The ratio, which is a measure of phase-space density, decays according to a power law, which signifies that a nonlinear process governs equilibration. This nonlinearity is reasonable since the rate of decay of the excess atoms should depend both on

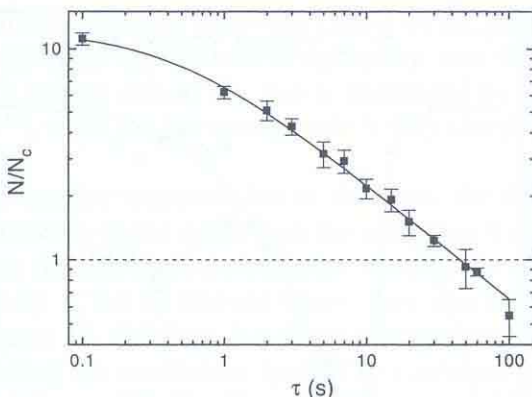


Figure 8. Relaxation of the gas to equilibrium following a rapid quench pulse at $\tau = 0$. The data from Fig. 5 was used to make this graph. The total number of atoms N and temperature T were used to determine N/N_c , where $N_c = 1.2(kT / \hbar\omega)^3$. The points represent averages of several measurements and the errors bars are standard deviations. The dashed line approximately denotes where equilibrium is reached. The solid line is an empirical fit. (Reprinted from Ref. 22).

the excess number and on the collision rate, which in turn depends on N and T . Since $N_0 \ll N$, equilibrium is reached when $N/N_c \approx 1$, which occurs at $\tau \approx 50$ s. This time is consistent with the delay required to accurately fit the image data with an equilibrium model, and with the results of the quantum Boltzmann model. Comparison of Figs. 5 and 8 shows that the equilibration time is also consistent with the changing shape of the measured histograms. This further strengthens the conclusion that the variations in N_0 are related to the growth and collapse of the condensate during the equilibration process, since the distribution of N_0 values changes when the population imbalance driving condensate growth is eliminated.

6. Molecular Spectroscopy of a Bose-Einstein Condensate

The ability to cool and trap atoms has enabled many new discoveries in many-body physics and in low-energy collision physics over the past few years. The same capabilities have not, however, been extended to molecules despite strong motivations to do so. Ultracold trapped molecules might, for example, lead to the extension of Bose-Einstein condensation to larger and more complex systems, or to the ability to coherently control chemical reactions. As with atoms, much greater understanding of interparticle interactions, both atom-molecule and molecule-molecule, could be gained through spectroscopic studies involving ultracold molecules.

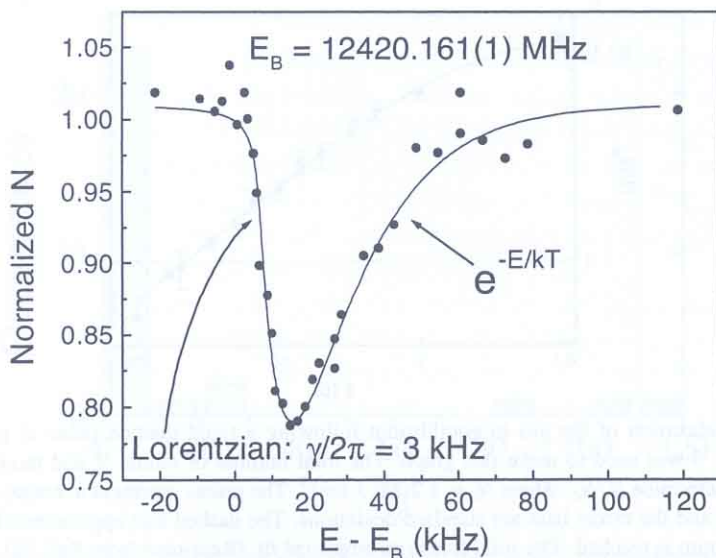


Figure 9. Two-photon photoassociation signal for total trap population. The total number of atoms remaining after a photoassociation pulse is normalized to measurements in the absence of photoassociation.

6.1. SPECTROSCOPY

One way to produce ultracold trapped molecules is to photoassociate ultracold trapped atoms. The two-photon technique used to determine the scattering lengths of lithium, shown in Fig. 1 can also be used for this purpose. The frequency difference $\omega_2 - \omega_1$ between the two lasers is tuned to the binding energy, E_B , of a vibrational level of the ground-state of the diatomic molecule. In the previous scattering length experiment, the gas was confined to a magneto-optical trap (MOT) at a temperature of 1 mK [6]. In the current experiment, the gas is much colder, $< 1 \mu\text{K}$, and has undergone Bose-Einstein condensation. Furthermore, since the new experiment is performed in a magnetic trap using spin-polarized atoms, any molecules that are produced will have magnetic moments, and therefore, may be trapped. A similar experiment was recently performed using a Bose-Einstein condensate of rubidium atoms, and the effect of atom-molecule interactions was observed in the molecular spectrum [36].

Since the atoms are extremely cold and the molecules may be relatively long-lived, the two-photon transition linewidth is potentially very narrow. In order to realize this potential sensitivity, two extended-cavity diode laser systems were phase-locked, with a resulting relative linewidth of under 1 Hz.

Fig. 9 shows a spectrum when $N \approx 10^6$ and $T \approx 700 \text{ nK}$. Under these conditions, the gas is quantum degenerate, although because of the attractive interactions, N_0 is always less than ~ 1250 atoms. The signal shown in Fig. 9 is the

total number of atoms remaining following a pulse of the photoassociating light. The spectrum is distinctly asymmetric. In agreement with the Wigner threshold law [37], the high energy side of the line is broadened by the thermal energy distribution, $e^{-E/kT}$, while the low-energy side is very sharp, having a linewidth of less than 3 kHz.

Fig. 10 shows another spectrum, but in this case, the signal is the number of remaining condensate atoms rather than the remaining total number. The gas is quenched before the photoassociation pulse, causing the condensate to grow. Since the condensate is fed by thermal atoms, they also contribute to the condensate signal. Figure 10, therefore, is a direct measurement of the entire energy distribution, including the condensate itself. The condensate peak is extremely narrow, its width being ~ 250 Hz. There are several possible sources of broadening. The laser beam of frequency ω_2 (Fig. 1) can induce a transition from the ground-state vibrational level, $v = 10$, to the vibrational level v' of the electronically excited state which serves as the intermediate state for the two-photon transition. Although the lasers are detuned by ≥ 100 MHz from this intermediate state, off-resonant excitation is possible, and spontaneous emission can occur. A second source of broadening arises from the mean-field interaction between the molecules and the inhomogeneously distributed atomic condensate [36]. And finally, the $v = 10$ level itself may be unstable due to vibrational relaxation collisions between molecules and atoms. The rate for this process has never been measured, and theoretical estimates are extremely difficult and are available only for collisions between H_2 and H [38]. From the observed width of the condensate feature, we obtain an upper limit of $2 \times 10^{-10} \text{ cm}^3 \text{ s}^{-1}$ for the rate constant for vibrational relaxation collisions between Li_2 ($v = 10$) and Li atoms.

6.2. DIRECT OBSERVATION OF GROWTH AND COLLAPSE

Since accurate measurements of small values of N_0 necessarily destroy the condensate, it has not been previously possible to observe the condensate dynamics in real time. However, we have now directly observed the initial growth and collapse of a Bose-Einstein condensate by using the two-photon transition to dump the condensate [39]. Because of the high spectral resolution of the two-photon transition, the condensate can be ‘surgically’ removed from the energy distribution, while only minimally affecting the thermal atoms. This synchronizes the growth and collapse cycles for different experiments at a particular point in time. The subsequent growth/collapse dynamics are then obtained by repeating the experiment and measuring N_0 at different delays following the dump pulse. In a recent experiment with essentially pure condensates of ^{85}Rb atoms, a magnetically tuned Feshbach resonance was used to suddenly switch the interactions from repulsive to attractive, thereby inducing a collapse at a specified time [40]. In that experiment, condensates are produced with N_0 far greater than the stability limit, and consequently with high initial energy. In contrast, for the present experiment, the

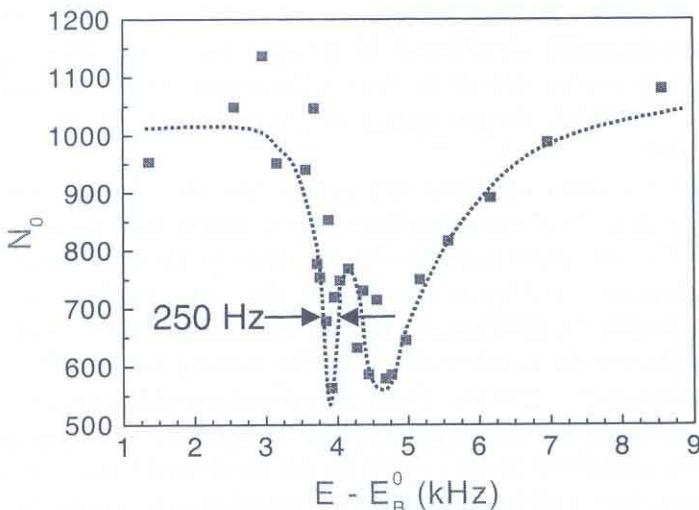


Figure 10. Two-photon photoassociation signal for condensate. The signal is number of remaining condensate atoms following a photoassociation pulse. The narrow peak at low-energy arises from probing the condensate directly.

collapse occurs with N_0 below the maximum number by macroscopic quantum tunneling or thermal fluctuation. Furthermore, the condensate coexists with a gas of thermal atoms, allowing the kinetics to be probed.

In order to stimulate rapid growth and collapse conditions, a 100 ms duration microwave quench pulse is applied following evaporative cooling. This pulse removes $\sim 80\%$ of the atoms, leaving all but the coldest $\sim 10^5$ atoms. This quench pulse leaves the gas far from thermal equilibrium, and if left to freely evolve, the condensate will alternately grow and collapse many times for a period of ~ 10 s, as shown in Fig. 6. After a delay of either 3 or 5 s following the microwave quench pulse, a light pulse consisting of two co-propagating laser beams tuned to the two-photon transition dumps the condensate. Once in the molecular state, the laser of frequency ω_2 can stimulate a single-photon transition to the intermediate level v' (Fig. 1), which can then spontaneously decay into a state of two energetic atoms that escape the trap. This method for removing atoms is very energy specific since the observed two-photon linewidth of 250 Hz is much less than the ~ 5 kHz thermal energy spread of the trapped atoms. In particular, the condensate may be selectively removed without significantly affecting the remaining atoms.

Following the light pulse, the gas is allowed to freely evolve for a certain time, at which point a destructive measurement of N_0 is made. Figure 11a shows the dynamical evolution of the condensate following a light pulse whose duration is adjusted to reduce N_0 to an initial value ~ 100 atoms. N_0 increases immediately after the light pulse as the condensate is fed via collisions between noncondensed thermal atoms, and N_0 reaches a maximum value consistent with the expected

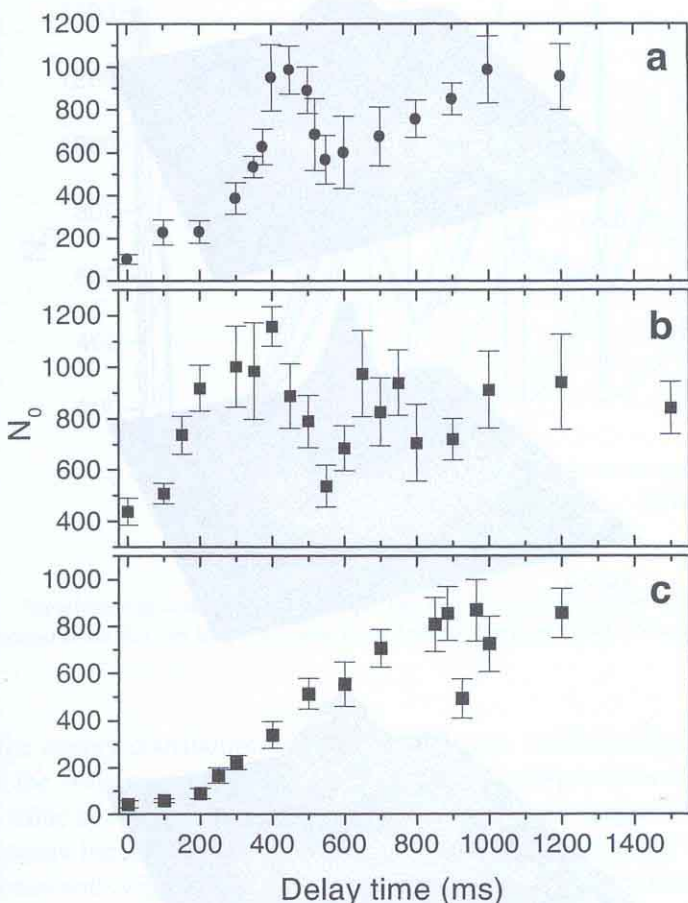


Figure 11. Condensate growth and collapse. (Reprinted from Ref. 39 by permission from Nature, copyright 2000, Macmillan Magazines Ltd.).

upper limit of 1250 atoms. A collapse is clearly indicated by the subsequent reduction in N_0 . After the collapse, N_0 grows again, since the gas is not yet in thermal equilibrium. The images shown in Fig. 12 are representative images taken from the data in Fig. 11a for the specified delay times. The central peak, most clearly visible at 450 ms delay, corresponds to the condensate.

The condensate growth rate may be adjusted by varying the duration of the light pulse. By reducing the duration, fewer atoms are removed from both the condensate and from the low-energy thermal atoms that directly contribute to condensate growth, and consequently the growth rate increases. This is shown in Fig. 11b, where two secondary peaks are now discernable. For Fig. 11c, the light pulse duration is lengthened, causing more atoms to be removed, and slowing the rate of growth.

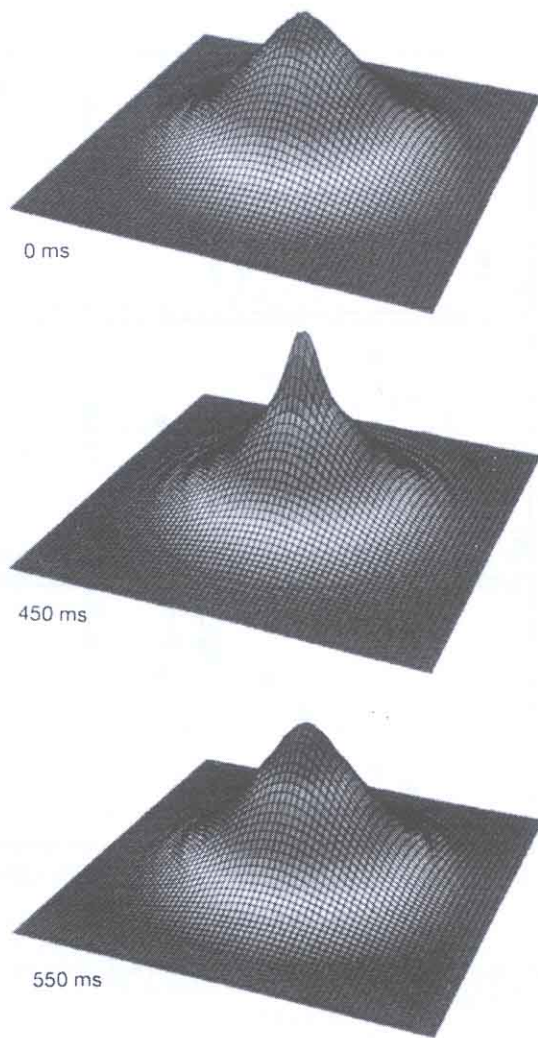


Figure 12. Phase-contrast images. These images were selected from those used to construct Fig. 11a. The fitted values of N_0 are 40, 1210, and 230 atoms for the upper, middle, and lower images, respectively. (Reprinted from Ref. 39 by permission from Nature, copyright 2000, Macmillan Magazines Ltd.).

Each data point in Fig. 11 is the mean of five separate measurements of N_0 . Consequently, these data represent an average of many trajectories whose initial phase and rate of growth differ slightly. The results are analyzed by using the quantum Boltzmann equation. The lighter curves shown in Fig. 13 are a sample of simulated trajectories which include the effect of the microwave quench pulse and the light pulse. The variation in condensate growth following the light pulse is mainly the result of slight differences in initial conditions that lead to varia-

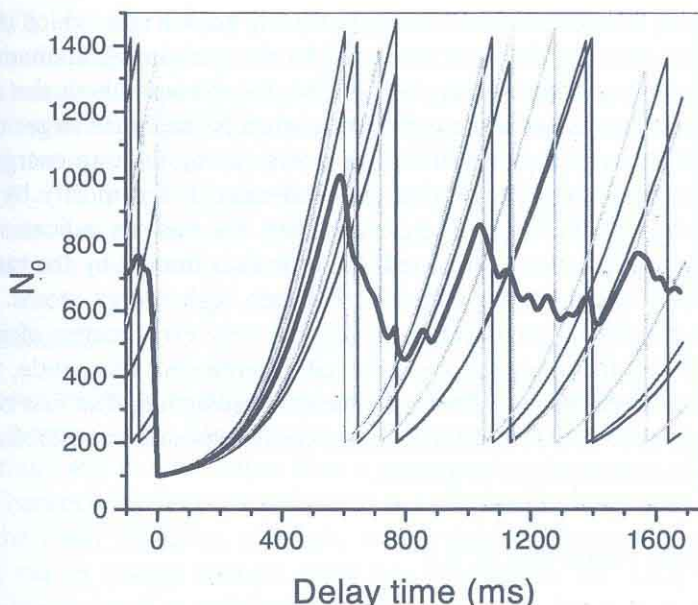


Figure 13. Simulation of condensate dynamics. The two-photon light pulse is applied at 0 delay time. (Reprinted from Ref. 39 by permission from Nature, copyright 2000, Macmillan Magazines Ltd.).

tions in the energy distribution of atoms in the trap. Additionally, the stochastic nature of the collapse process, which causes each collapse to occur at a slightly different value of N_0 , contributes to dephasing of different trajectories. The heavy line represents the average of 40 trajectories obtained by running the simulation several times with slightly different initial conditions. In the simulations, N_0 is set to 200 atoms immediately following the light pulse in order to achieve the best agreement with the histograms of Fig. 5. The only adjustable parameter in the simulations is the fraction of thermal atoms lost within the spectral width of the two-photon transition.

The simulation results agree well with the data in several respects. The data in Fig. 11b show that each subsequent peak following the initial growth is slightly lower, as the trajectories corresponding to each individual measurement dephase from one another. This dephasing causes the maxima (minima) to occur at smaller (larger) values of N_0 than for any individual trajectory. This behavior is seen in the simulation average shown in Fig. 13, confirming our understanding of the role of averaging in these measurements.

6.3. GROWTH OF THE CONDENSATE

Condensate growth should be affected by the quantum statistical effect known as Bose enhancement: the condensate growth rate scales with the occupation number

N_0 . This would lead to an exponentially increasing growth rate, which is, however, neither observed in the data nor predicted by the quantum Boltzmann equation model. For the conditions shown in Fig. 11c, for example, both the model and the data show a saturation in the growth rate when N_0 becomes larger than ~ 150 atoms. An analysis of the distribution of atoms among the trap energy levels in the model simulations indicates that the condensate is fed mostly by collisions between atoms with the lowest energies. Further, this analysis indicates that when the low-energy population is depleted, the growth is limited by the rate for non-Bose-enhanced ‘trickle-down’ collisions between high-energy atoms. Owing to our high sensitivity to small values of N_0 , the very early stages of condensate growth following the dump can be observed, illuminating this subtle, yet important, departure from the pure Bose enhancement prediction. The first observation of condensate growth [35] could not detect small values of and therefore was not sensitive to the initial stages of growth.

7. Degenerate Fermi Gas of ^6Li

An exciting new direction in the ultra-cold atom field is to study a quantum degenerate gas composed of fermions rather than bosons. A gas of fermionic ^{40}K atoms has recently been cooled to degeneracy [41]. We have initiated an experiment to produce an ultra-cold gas of fermionic ^6Li atoms. As with the Bose gases, much of the interesting physics has to do with the interactions between atoms. ^6Li is particularly intriguing because, by a fluke of nature, the interaction between two atoms is enormously large and attractive (Table I) [7], enabling perhaps, the first observation of a Bardeen-Cooper-Schrieffer (BCS) phase transition to a gaseous superfluid state [42, 43].

7.1. BCS PHASE-TRANSITION

The BCS theory was developed to explain superconductivity and has also been applied to superfluid ^3He . The fundamental effect underlying these phenomena is the pairing of particles, known as ‘Cooper pairing’. In 1980, Leggett considered whether such a transition could be observed in a deuterium gas [44]. He showed that the transition temperature $T_c \approx (5E_F/3k_B) \exp[-\pi / (2k_F|a|) - 1]$, where E_F is the Fermi energy, k_F is the Fermi wave number, and a is the s -wave scattering length ($a \approx -7a_0$), is way too low for there to be any hope of seeing the transition in the gas phase in deuterium. However, Stoof et al. recently pointed out that ^6Li is the ideal candidate for such an experiment, given that a is over 300 times larger than for deuterium (Table I) [42, 43]. With 200,000 atoms, a number with which we are able to produce degenerate gases of ^7Li , the simple expression above gives an experimentally achievable $T_c \approx 25$ nK. Because of the Pauli principle, realization of s -wave pairing requires a mixture of two spin-states.

The $F = 3/2, m_F = 3/2$ and $F = 3/2, m_F = 1/2$ mixture is one possibility as it interacts via the large triplet scattering length. However, this mixture is unstable to spin-exchange collisions for reasonable magnetic field strengths [42]. We intend instead to use a magnetically-tuned Feshbach resonance to tune the sign and strength of the resonance. The energetically lowest two states of the hyperfine manifold, $F = 12, m_F = 12$ plus $F = 12, m_F = -12$, and the second and third lowest states, $F = 12, m_F = -12$ plus $F = 3/2, m_F = -3/2$, are predicted to exhibit Feshbach resonances near 800 G [45].

7.2. EXPERIMENT

The apparatus and techniques that we use to produce a degenerate gas of ${}^6\text{Li}$ are similar to those used for ${}^7\text{Li}$ (Section 3), except that a cloverleaf-type electromagnetic trap [46] is used rather than a permanent magnet trap. The primary difference between the boson experiments and the fermion experiment arises because of the Pauli exclusion principle, which forbids identical fermions from interacting via an s-wave channel. This fact complicates the usual evaporative cooling technique used so successfully with Bose gases, because of the inability of identical fermions to undergo the necessary thermalization collisions. We circumvent this difficulty by cooling the ${}^6\text{Li}$ atoms ‘sympathetically’ [47, 48] via their interactions with evaporatively cooled ${}^7\text{Li}$ atoms. This adds complexity to the experiment because both isotopes must be simultaneously trapped.

We have recently cooled magnetically trapped ${}^6\text{Li}$ atoms below the Fermi temperature. The magnetic trap is loaded by transferring both ${}^6\text{Li}$ and ${}^7\text{Li}$ atoms from a dual species magneto-optical trap (MOT), which in turn is loaded from a laserslowed thermal atomic beam using the Zeeman slowing technique [49]. Approximately $10^{10} {}^7\text{Li}$ atoms and $10^8 {}^6\text{Li}$ atoms are loaded into the MOT at a temperature of 500 μK . Of these, $\sim 10\%$ are transferred to the magnetic trap. Fig. 14 shows absorption images of ${}^7\text{Li}$ on the left and ${}^6\text{Li}$ on the right. Although the number of atoms is different, each image corresponds to temperatures of somewhat less than T_F . The time between corresponding ${}^6\text{Li}$ and ${}^7\text{Li}$ images is less than 1 s. The spatial size of the ${}^6\text{Li}$ atom cloud is distinctly larger than the ${}^7\text{Li}$ cloud, especially at the lowest temperature. Other than the 15% difference in trap frequency between the isotopes, the size difference might be a manifestation of quantum statistics, which tends to shrink the Bose distribution, while enlarging the Fermi distribution.

7.3. FUTURE EXPERIMENTS

Realization of the BCS phase-transition will require the atoms to be cooled far below T_F . Our plan is to transfer the magnetically trapped ${}^6\text{Li}$ atoms to an optical dipole trap in the lowest two hyperfine levels. The ${}^7\text{Li}$ atoms can be first removed using a microwave spin-flip transition. Once in the optical trap and in the two-

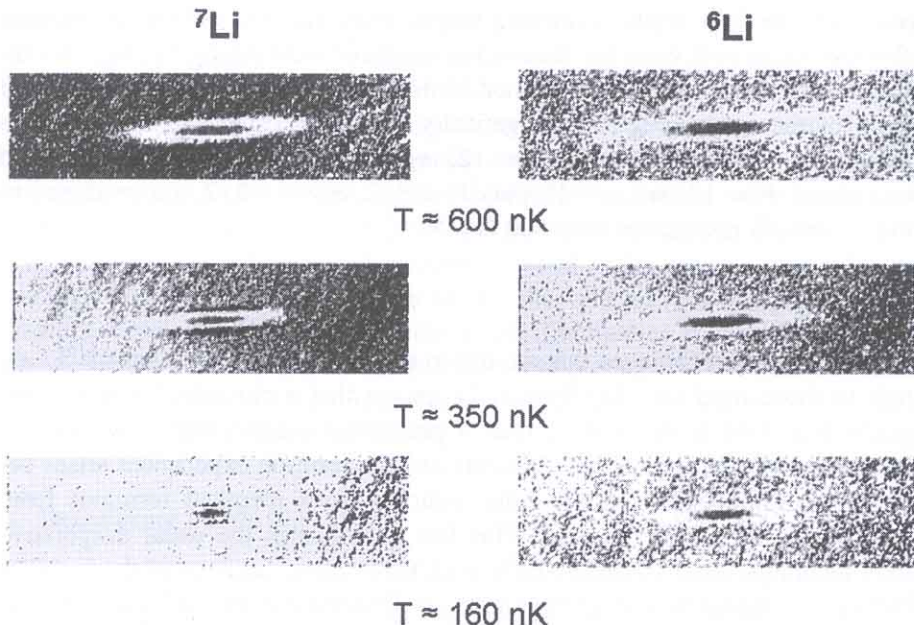


Figure 14. Sympathetic cooling of fermionic ${}^6\text{Li}$ below T_F . The ${}^7\text{Li}$ is evaporatively cooled while the ${}^6\text{Li}$ is sympathetically cooled via collisions with ${}^7\text{Li}$. The three different temperatures correspond to three separate evaporation cycles. A separate laser beam is used to image each isotope.

state mixture, the ${}^6\text{Li}$ atoms can be directly evaporated by lowering the optical potential.

There are several possible manifestations of the BCS phase-transition that we will look to as signatures, but there is opportunity for much more theoretical work to fully understand the implications. Perhaps the best possibility is to optically detect the presence of Cooper pairs [50, 51, 52]. Our idea is to image the Fourier plane of the density distribution of the gas, which should be sensitive to the momentum pair-distribution function [50]. Calculations show that the length scale of the pair correlation function is much smaller than the size of the trapped atom cloud. The presence of pairs should result in large angle scattering that could be detected using the usual imaging techniques developed to image Bose-Einstein condensates of trapped atoms.

8. Conclusions and Outlook

The opportunity to study quantum degenerate gases is very exciting. The isotopes of lithium are particularly interesting because the bosonic isotope has attractive

interactions, which lead to collective collapse, while the fermionic isotope has an enormously large attractive interaction, which may provide the means to observe a BCS phase transition to a gaseous superfluid state.

Acknowledgements

The authors wish to thank Ian McAlexander, Ionut Prodan, Cass Sackett, Kevin Strecker, Dmitry Strekalov, and Andrew Truscott for their contributions to the research described here. We are grateful to the NSF, NASA, ONR, and the Welch Foundation for their support.

References

1. Bradley, C.C., Sackett, C.A., Tollett, J.J., and Hulet, R.G. (1995) Evidence of Bose-Einstein Condensation in an Atomic Gas with Attractive Interactions, *Phys. Rev. Lett.* **75**, 1687.
2. Huang, K. (1987). *Statistical Mechanics*, John Wiley and Sons, New York.
3. Fried, D.G., Killian, T.C., Willmann, L., Landhuis, D., Moss, S.C., Kleppner, D., and Gretyak, T.J. (1998) Bose-Einstein condensation of atomic hydrogen, *Phys. Rev. Lett.* **81**, 3811-3814.
4. Dalfovo, F., Giorgini, S., Pitaevskii, L.P., and Stringari, S. (1999) Theory of Bose-Einstein condensation in trapped gases, *Rev. Mod. Phys.* **71**, 463-512.
5. Weiner, J., Bagnato, V., Zilio, S., and Julienne, P.S. (1999) Experiments and Theory in Cold and Ultracold Collisions, *Rev. Mod. Phys.* **71**, 1-85.
6. Abraham, E.R.I., McAlexander, W.I., Sackett, C.A., and Hulet, R.G. (1995) Spectroscopic Determination of the S-Wave Scattering Length of Lithium, *Phys. Rev. Lett.* **74**, 1315-1318.
7. Abraham, E.R.I., McAlexander, W.I., Gerton, J.M., Hulet, R.G., Cote, R., and Dalgarno, A. (1997) Triplet s-wave resonance in ${}^6\text{Li}$ collisions and scattering lengths of ${}^6\text{Li}$ and ${}^7\text{Li}$, *Phys. Rev. A* **55**, R3299-3302.
8. Tsai, C.C., Freeland, R.S., Vogels, J.M., Boesten, H.M.J.M., Verhaar, B.J., and Heinzen, D.J. (1997) Two-Color Photoassociation Spectroscopy of Ground State Rb_2 , *Phys. Rev. Lett.* **79**, 1245-1248.
9. Bogoliubov, N. (1947) On the Theory of Superfluidity, *Journal of Physics (USSR)* **11**, 23-32.
10. Stoof, H.T.C. (1994) Atomic Bose gas with a negative scattering length, *Phys. Rev. A* **49**, 3824-3830.
11. Bradley, C.C., Sackett, C.A., and Hulet, R.G. (1997) Bose-Einstein Condensation of Lithium: Observation of Limited Condensate Number, *Phys. Rev. Lett.* **78**, 985-989.
12. Ruprecht, P.A., Holland, M.J., Burnett, K., and Edwards, M. (1995) Time-dependent solution of the nonlinear Schrodinger equation for Bose-condensed trapped neutral atoms, *Phys. Rev. A* **51**, 4704.
13. Sackett, C.A., Bradley, C.C., Welling, M., and Hulet, R.G. (1997) Bose-Einstein Condensation of Lithium, *Appl. Phys. B* **65**, 433-440.
14. Baym, G. and Pethick, C.J. (1996) Ground-State Properties of Magnetically Trapped Bose-Condensed Rubidium Gas, *Phys. Rev. Lett.* **76**, 6-9.
15. Stoof, H.T.C. (1997) Macroscopic Quantum Tunneling of a Bose Condensate, *J. Stat. Phys.* **87**, 1353-1366.
16. Tollett, J.J., Bradley, C.C., Sackett, C.A., and Hulet, R.G. (1995) Permanent Magnet Trap for Cold Atoms, *Phys. Rev. A* **51**, R22-R25.

17. P rez-Garc a, V., Michinel, H., Cirac, J.I., Lewenstein, M., and Zoller, P. (1997) Dynamics of Bose-Einstein condensates: Variational solutions of the Gross-Pitaevskii equations, *Phys. Rev. A* **56**, 1424-1432.
18. Sackett, C.A., Bradley, C.C., and Hulet, R.G. (1997) Optimization of Evaporative Cooling, *Phys. Rev. A* **55**, 3797.
19. Gerton, J.M., Sackett, C.A., Frew, B.J., and Hulet, R.G. (1999) Dipolar relaxation collisions in magnetically trapped ^7Li , *Phys. Rev. A* **59**, 1514-1516.
20. Bradley, C.C., Sackett, C.A., and Hulet, R.G. (1997) Analysis of In Situ Images of Bose-Einstein Condensates of Lithium, *Phys. Rev. A* **55**, 3951.
21. Sackett, C.A., Stoof, H.T.C., and Hulet, R.G. (1998) Growth and Collapse of a Bose Condensate with Attractive Interactions, *Phys. Rev. Lett.* **80**, 2031-2034.
22. Sackett, C.A., Gerton, J.M., Welling, M., and Hulet, R.G. (1999) Measurements of Collective Collapse in a Bose-Einstein Condensate with Attractive Interactions, *Phys. Rev. Lett.* **82**, 876.
23. Kagan, Y., Shlyapnikov, G.V., and Walraven, J.T.M. (1996) Bose-Einstein Condensation in Trapped Atomic Gases, *Phys. Rev. Lett.* **76**, 2670-2673.
24. Shuryak, E.V. (1996) Bose Condensate made of Atoms with Attractive Interaction is Metastable, *Phys. Rev. A* **54**, 3151.
25. Ueda, M. and Leggett, A.J. (1998) Macroscopic Quantum Tunneling of a Bose-Einstein Condensate with Attractive Interactions, *Phys. Rev. Lett.* **80**, 1576.
26. Huepe, C., M tens, S., Dewel, G., Borckmans, P., and Brachat, M.E. (1999) Decay Rates in Attractive Bose-Einstein Condensates, *Phys. Rev. Lett.* **82**, 1616-1619.
27. Singh, K.G., and Rokhsar, D.S. (1996) Collective Excitations of a Confined Bose Condensate, *Phys. Rev. Lett.* **77**, 1667-1670.
28. Dodd, R.J., Edwards, M., Williams, C.J., Clark, C.W., Holland, M.J., Ruprecht, P.A., and Burnett, K. (1996) Role of attractive interactions on Bose-Einstein condensation, *Phys. Rev. A* **54**, 661-664.
29. Kagan, Y., Muryshev, A.E., and Shlyapnikov, G.V. (1998) Collapse and Bose-Einstein Condensation in a Trapped Bose Gas with Negative Scattering Length, *Phys. Rev. Lett.* **81**, 933-937.
30. Houbiers, M., and Stoof, H.T.C. (1996) Stability of Bose condensed atomic ^7Li , *Phys. Rev. A* **54**, 5055.
31. Chandrasekhar, S. (1957) *An Introduction to the Study of Stellar Structure*, Dover, New York.
32. Zhakharov, V.E. (1972) Collapse of Langmuir Waves, *Sov. Phys. JETP* **35**, 908.
33. Zhakharov, V.E., and Synakh, V.S. (1975) The nature of the self-focusing singularity, *Sov. Phys. JETP* **41**, 465.
34. Gammal, A., Frederico, T., Tomio, L., and Chomaz, P. (2000) Atomic Bose-Einstein condensation with three-body interactions and collective excitations, *J. Phys. B* **33**, 4053-4067.
35. Miesner, H.-J., Stamper-Kurn, D.M., Andrews, M.R., Durfee, D.S., Inouye, S., and Ketterle, W. (1998) Bosonic Stimulation in the Formation of a Bose-Einstein Condensate, *Science* **279**, 1005-1007.
36. Wynar, R., Freeland, R.S., Han, D.J., Ryu, C., and Heinzen, D.J. (2000) Molecules in a Bose-Einstein Condensate, *Science* **287**, 1016-1019.
37. Napolitano, R., Weiner, J., Williams, C.J., and Julienne, P.S. (1994) Line Shapes of High Resolution Photoassociation Spectra of Optically Cooled Atoms, *Phys. Rev. Lett.* **73**, 1352-1355.
38. Forrey, R.C., Kharchenko, V., Balakrishnan, N., and Dalgarno, A. (1999) Vibrational relaxation of trapped molecules, *Phys. Rev. A* **59**, 2146-2152.
39. Gerton, J.M., Strekalov, D., Prodan, I., and Hulet, R.G. (2000) Direct observation of growth and collapse of a Bose-Einstein condensate with attractive interactions, *Nature* **408**, 692-695.
40. Cornish, S.L., Claussen, N.R., Roberts, J.L., Cornell, E.A., and Wieman, C.E. (2000) Stable

- ⁸⁵Rb Bose-Einstein condensates with widely tunable interactions, *Phys. Rev. Lett.* **85**, 1795-1798.
- 41. DeMarco, B., and Jin, D.S. (1999) Onset of Fermi degeneracy in a trapped atomic gas, *Science* **285**, 1703.
 - 42. Stoof, H.T.C., Houbiers, M., Sackett, C.A., and Hulet, R.G. (1996) Superfluidity of Spin-Polarized ⁶Li, *Phys. Rev. Lett.* **76**, 10.
 - 43. Houbiers, M., Ferwerda, R., Stoof, H.T.C., McAlexander, W.I., Sackett, C.A., and Hulet, R.G. (1997) The Superfluid State of Atomic ⁶Li in a Magnetic Trap, *Phys. Rev. A* **56**, 4864-4878.
 - 44. Leggett, A.J. (1980) Cooper Pairing in Spin-Polarized Fermi Systems, *J. Phys. (Paris) C* **7**, 19.
 - 45. Houbiers, M., Stoof, H.T.C., McAlexander, W.I., and Hulet, R.G. (1998) Elastic and inelastic collisions of ⁶Li atoms in magnetic and optical traps, *Phys. Rev. A* **57**, R1497-1500.
 - 46. Mewes, M.-O., Andrews, M.R., van Druten, N. J., Kurn, D.M., Durfee, D.S., and Ketterle, W. (1996) Bose-Einstein Condensation in a Tightly Confining dc Magnetic Trap, *Phys. Rev. Lett.* **77**, 416-419.
 - 47. Larson, D.J., Bergquist, J.C., Bollinger, J.J., Itano, W.M., and Wineland, D.J. (1986) Sympathetic Cooling of Trapped Ions: A Laser-Cooled Two-Species Nonneutral Ion Plasma, *Phys. Rev. Lett.* **57**, 70-73.
 - 48. Myatt, C.J., Burt, E.A., Christ, R.W., Cornell, E.A., and Wieman, C.E. (1997) Production of Two Overlapping Bose-Einstein Condensates by Sympathetic Cooling, *Phys. Rev. Lett.* **78**, 586-589.
 - 49. Phillips, W.D., and Metcalf, H. (1982) Laser Deceleration of an Atomic Beam, *Phys. Rev. Lett.* **48**, 596-599.
 - 50. Zhang, W., Sackett, C.A., and Hulet, R.G. (1999) Optical detection of a Bardeen-Cooper-Schrieffer phase transition in a trapped gas of fermionic atoms, *Phys. Rev. A* **60**, 504-507.
 - 51. Ruostekoski, J. (1999) Optical response of a superfluid state in dilute atomic Fermi-Dirac gases, *Phys. Rev. A* **60**, R1775-1778.
 - 52. Torma, P., and Zoller, P. (2000) Laser Probing of Atomic Cooper Pairs, *Phys. Rev. Lett.* **85**, 487-90.